Photoneutron cross sections for Mo isotopes: A step toward a unified understanding of (γ,n) and (n,γ) reactions

H. Utsunomiya,[1] S. Goriely,[2] T. Kondo,[1] C. Iwamoto,[1] H. Akimune,[1] T. Yamagata,[1] H. Toyokawa,[3] H. Harada,[4] F. Kitatani,[4] Y.-W. Lui,[5] A. C. Larsen,[2,6] M. Guttormsen,[2,6] P. E. Koehler,[6] S. Hilaire,[7] S. Péru,[7] M. Martini,[2,7] and A. J. Koning[8]

[1]*Department of Physics, Konan University, Okamoto 8-9-1, Higashinada, Kobe 658-8501, Japan*

[2]*Institut d'Astronomie et d'Astrophysique, Université Libre de Bruxelles, Campus de la Plaine, CP-226, 1050 Brussels, Belgium*

[3]*National Institute of Advanced Industrial Science and Technology, Tsukuba 305-8568, Japan*

[4]*Japan Atomic Energy Agency, Tokai-mura, Naka, Ibaraki 319-1195, Japan*

[5]*Cyclotron Institute, Texas A&M University, College Station, Texas 77843, USA*

[6]*Department of Physics, University of Oslo, N-0316 Oslo, Norway*

[7]*CEA, DAM, DIF, F-91297 Arpajon, France*

[8]*Nuclear Research and Consultancy Group, P.O. Box 25, NL-1755 ZG Petten, The Netherlands*

(Received 7 May 2013; published 15 July 2013)

Photoneutron cross sections were measured for ^{94}Mo, ^{95}Mo, ^{96}Mo, ^{97}Mo, ^{98}Mo, and ^{100}Mo near the neutron threshold with quasi-monochromatic laser-Compton scattering γ rays. The photoneutron data were analyzed with the Skyrme Hartree-Fock-Bogoliubov (HFB) plus quasiparticle random phase approximation (QRPA) model and the axially symmetric-deformed Gogny HFB plus QRPA model of $E1$ γ-ray strength. Combining the γ-ray strength function constrained by the present photoneutron data with either the nuclear resonance fluorescence data or the updated Oslo data to supplement the data below the neutron threshold, a thorough analysis of the reverse (n,γ) cross sections is made whenever measurements are available. The Oslo data and the corresponding uncertainties are updated based on the latest results of the s-wave neutron spacing and the average radiative width determined in particular for ^{96}Mo. Finally, radiative neutron capture cross sections for two radioactive nuclei, ^{93}Mo and ^{99}Mo, are deduced with the γ-ray strength function method.

DOI: 10.1103/PhysRevC.88.015805 PACS number(s): 25.20.Lj, 21.10.Pc, 25.40.Lw, 27.60.+j

I. INTRODUCTION

Photoneutron cross sections and radiative neutron capture cross sections are fundamental nuclear inputs to stellar model calculations of the s-, r-, and p-process nucleosynthesis. A comprehensive understanding of (γ,n) and (n,γ) cross sections requires a knowledge of nuclear statistical quantities such as the γ-ray strength function (γSF) and the nuclear level density. The γSF is the quantity which interconnects photoneutron emission and radiative neutron capture, thus, is a key to the Hauser-Feshbach model calculations of both (n,γ) and (γ,n) cross sections. As discussed in [1,2], the γSF plays an important role in both nuclear astrophysics and nuclear engineering. Photoneutron cross sections, hence the γSF, immediately above neutron threshold is of direct relevance to the p-process nucleosynthesis which transforms pre-existing seed nuclei produced by the s- and r-process nucleosynthesis into neutron-deficient nuclei classified as p-process nuclei [3–5]. In contrast, the γSF below the neutron threshold plays a key role in defining the electromagnetic de-excitation taking place after the neutron capture which, along with the β decay, drives the s- and r-process nucleosynthesis [6,7].

The γ-ray strength function for six molybdenum isotopes, $^{93-98}$Mo, has been investigated with the Oslo method using (^{3}He, ^{3}He$'\gamma$) and (^{3}He, $\alpha\gamma$) reactions [8], while electric dipole strength has been investigated for five even-mass Mo isotopes, ^{92,94,96,98,100}Mo, and magnetic dipole strength for three isotopes, ^{92,98,100}Mo, in nuclear resonance fluorescence experiments [9–11].

In this paper, we present experimental photoneutron cross sections for ^{94,95,96,97,98,100}Mo near the neutron threshold among which those for two odd-N isotopes, ^{95}Mo and ^{97}Mo, are presented here for the first time. We systematically discuss (γ,n) and (n,γ) cross sections for molybdenum isotopes in the context of the γ-ray strength function (γSF) method [1,2]. The photoneutron emission and radiative neutron capture on Mo isotopes of interest in the present paper are depicted in Fig. 1. The neutron thresholds even for the two odd-N nuclei were not low enough to directly detect extra low-energy strength in the photoneutron channel. However, combining the γSF constrained by the present data with the low-energy data derived from either the (γ,γ') [9,10] or the Oslo [8] experiments (updated with the latest results of the s-wave resonance spacing and the average γ-decay width [12]) enables us to analyze (n,γ) cross sections for stable Mo isotopes systematically. The photoneutron data and the γSF for ^{95}Mo and ^{94}Mo are of direct relevance to the production and destruction of ^{94}Mo, respectively, in the p-process nucleosynthesis though there is a well-known issue of the underproduction of ^{92,94}Mo and ^{96,98}Ru in this mass region of the chart of nuclei [3]. With the γ-ray strength function method, we indirectly determine (n,γ) cross sections for two radioactive Mo isotopes, ^{93}Mo with the half-life 4×10^3 yr and ^{99}Mo with the half-life 2.75 d, which constitute nuclear inputs for the reaction network calculations for the p and s process, respectively.

II. PHOTONEUTRON CROSS SECTION MEASUREMENTS

The experiment was performed with quasi-monochromatic laser-Compton scattering (LCS) γ rays at the National Institute of Advanced Industrial Science and Technology (Japan).

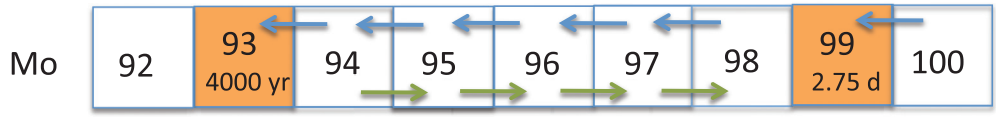

FIG. 1. (Color online) The chart of nuclei depicting our systematic analysis of (γ,n) and (n,γ) cross sections for Mo isotopes in the context of the γ-ray strength function method. Photoneutron cross sections measured in the present experiment are shown by left arrows. Radiative neutron capture cross sections discussed in the present systematic analysis are shown by right arrows. Photoneutron cross sections for two radioactive nuclei, ^{93}Mo and ^{99}Mo, are deduced with the γ-ray strength function method.

The present measurement for molybdenum isotopes was made in parallel to that for tin isotopes [13] in the same experiment. Therefore, we restrict ourselves to the description of the experimental procedure specific to the measurement for molybdenum isotopes, while other details can be found in Refs. [1,13].

The LCS γ rays were produced in an energy range from 7.55 MeV to 13.00 MeV (the quoted energy represents the maximum energy of the LCS γ-ray beam) with a high-intensity Nd:YVO_4 Q-switch laser. Enriched metal powders of ^{94}Mo (98.97%, 1921 mg), ^{95}Mo (94.38%, 1992 mg), ^{96}Mo (95.9%, 2001 mg), ^{97}Mo (91.7%, 999 mg), ^{98}Mo (98.55%, 1749 mg), and ^{100}Mo (99.27%, 2850 mg) were pressed/shaped into targets of 8 mm diameter and 16–19 mm lengths.

Measurements below the neutron threshold S_n were carried out for ^{94}Mo ($S_n = 9.68$ MeV) at 9.50 MeV, ^{96}Mo ($S_n = 9.15$ MeV) at 9.00 MeV, and ^{100}Mo ($S_n = 8.29$ MeV) at 8.25 MeV with no significant neutron events observed. The LCS γ-ray beam was measured with the high-resolution high-energy photon spectrometer [14] at a reduced laser power to determine the energy distributions of the LCS γ-ray beam by means of the unfolding technique [15,16]. Figure 2 shows an example of the unfolded energy spectra of the incident γ-ray beams.

Photoneutron cross sections were deduced at the average γ-ray energies with the Taylor expansion method [1]. The systematic uncertainty for the cross section is ±4.4%, which represents a quadratic sum of uncertainties of the neutron detection efficiency (3.2%) and the number of incident γ rays (3%). The final cross sections are shown in Fig. 3 and compared with previous measurements when available.

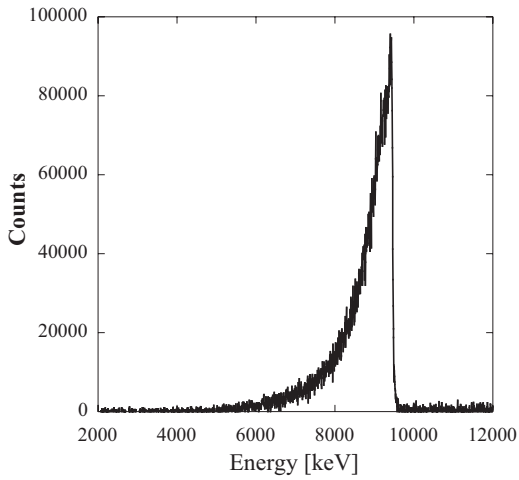

FIG. 2. A typical energy distribution of the LCS γ-ray beam used in the present experiment.

III. COMPARISON WITH THEORETICAL PREDICTIONS AND AUXILIARY DATA

The photoneutron cross-section data have been compared to theoretical calculations on the basis of the TALYS nuclear reaction code [19] and two different models of the γSF, namely the Skyrme HFB plus QRPA model [20] based on the BSk7 interaction, and the axially symmetric-deformed Gogny HFB plus QRPA model based on the D1M interaction [21–23]. Both models are based on the QRPA approach but make use of different interactions. The BSk7 + QRPA model is based on the BSk7 Skyrme force where some phenomenological corrections are introduced to take the damping of the collective motion as well as the deformation effects into account. In contrast to the Skyrme-based model, the D1M + QRPA model allows for a consistent description of axially symmetric deformations and includes phenomenologically the impact of multiparticle multihole configuration as a function of their densities [23]. Both models have proven their capacity to reproduce experimental photoabsorption data relatively well. As seen in Fig. 3, cross sections around the neutron threshold are rather well described by the HFB + QRPA models, although some deviations can be seen. Note that no renormalization of the strength has been performed for these calculations. In contrast to other cases, see for example Ref. [1], the agreement around the neutron threshold is rather satisfactory and there is no reason to invoke the presence of extra low-lying strength from the present data, at least in the vicinity of the neutron threshold.

Below the neutron threshold, additional experimental information exists; this includes the (γ,γ') measurements on ^{92,94,96,98,100}Mo [10,24], and the analysis of particle-γ coincidence data on $^{93-98}$Mo from neutron pickup (^{3}He,$\alpha\gamma$) and/or inelastic scattering (^{3}He,^{3}He$'\gamma$) reactions [8,25]. As shown in Figs. 4 and 5, such measurements cover a rather large range of energies below the neutron threshold. However, the shape and absolute value of the γSF from the two measurements seem to be contradictory. One should keep in mind that both methods are affected by rather large model-dependent uncertainties, although those might not be reflected in the quoted error bars, which typically show statistical errors only. It is interesting to note that for ^{95}Mo, the overall shape of the γSF extracted with the Oslo method is in excellent agreement with recent $(d, p\gamma)^{95}$Mo data from Ref. [26].

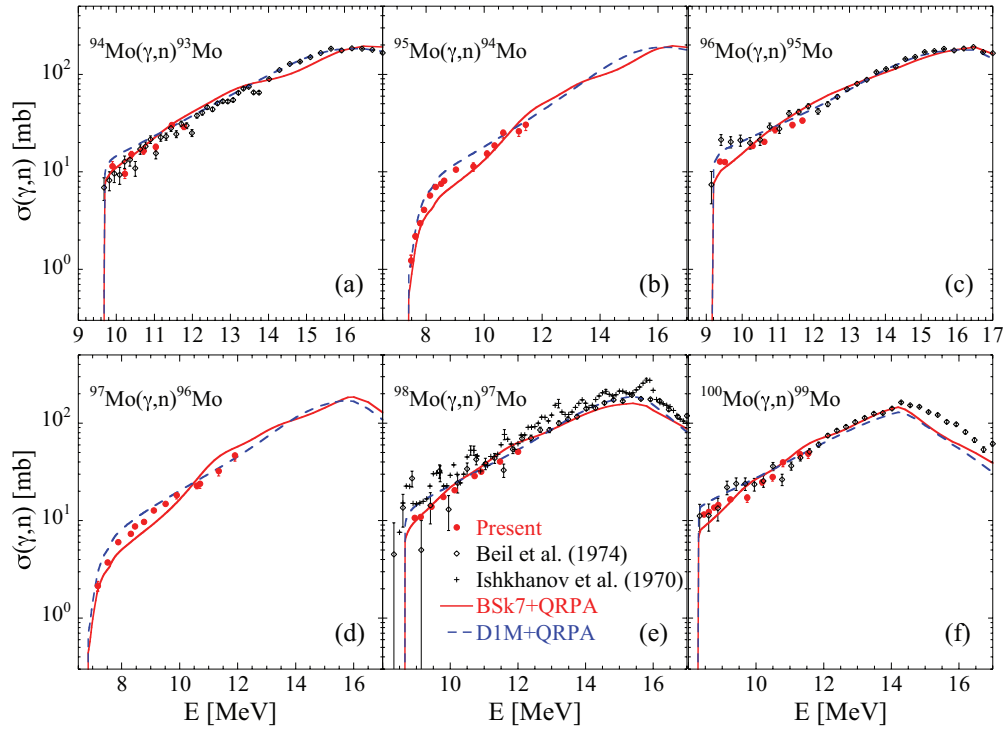

FIG. 3. (Color online) Comparison between the present photoneutron emission cross sections and previously measured ones [17,18] for six Mo isotopes, ^{94}Mo (a), ^{95}Mo (b), ^{96}Mo (c), ^{97}Mo (d), ^{98}Mo (e), and ^{100}Mo (f). Also included are the predictions from Skyrme HFB + QRPA (based on the BSk7 interaction) [20] and axially deformed Gogny HFB + QRPA models (based on the D1M interaction) [23].

To determine the γSF within the Oslo method, data on the s-wave resonance spacing D_0 and the average, total radiative width $\langle\Gamma_\gamma\rangle$ from neutron-resonance experiments are essential for the normalization procedure (see Ref. [27] for a more detailed description of the method, and Ref. [28] for a thorough analysis of possible systematic errors). In the original normalization [8], the values recommended by the RIPL library [29] were considered. However, a detailed analysis of a new ^{95}Mo$(n,\gamma)^{96}$Mo measurement [12,30] shows a significant deviation from the RIPL D_0 and $\langle\Gamma_\gamma\rangle$ values, more specifically D_0 is reduced by 63% and $\langle\Gamma_\gamma\rangle$ is increased by 25%. The corresponding error bars are rather small (see Table I) due to the large number of resonances available in the new experiment. Since such a detailed analysis is not available for the other Mo isotopes, we assume that the corresponding RIPL D_0 and $\langle\Gamma_\gamma\rangle$ values are affected by similar uncertainties. For this reason, we have adopted a similar uncertainty range for the other Mo isotopes for which Oslo data are available, as summarized in Table I (for ^{98}Mo additional information from Ref. [31] also reduce the corresponding uncertainties). Those uncertainties are responsible for the large error bars shown in Figs. 4 and 5, especially when the D_0 value is not well constrained. Note that the error bars shown in these figures include statistical uncertainties for the Oslo data sets and uncertainties in the D_0 and $\langle\Gamma_\gamma\rangle$ values.

Regarding the (γ,γ') data [10,24], the systematic errors are not so transparent. However, considering uncertainties due to the applied level density models as shown in Fig. 17 of Ref. [10], the systematic error is at least a factor of 2. In addition, there are possible systematic errors due to assumptions of the input γSF model and the equal-parity distribution applied in the correction procedure to estimate missing quasicontinuum strength.

Finally from Figs. 3–5, it can be seen that even if there is no reason to invoke the presence of some extra strength above the neutron threshold with respect to the QRPA predictions, below the threshold, some pygmy resonances, as observed for example for the Sn isotopes [13], may still be required to explain the (γ,γ') data, in particular in ^{94,96,98}Mo. The D1M + QRPA model systematically predicts larger $E1$ strength below the neutron threshold than the BSk7 + QRPA one and is also seen to be in better agreement with data in this energy region.

IV. RADIATIVE NEUTRON CAPTURE AND THE γSF METHOD

We now turn to the reverse radiative neutron capture channel. It should be kept in mind that the corresponding cross section for incident keV neutrons depends sensitively on the γSF, but in a rather lower energy range below the neutron threshold, typically around 6 MeV of γ-ray energy.

On the basis of the γ-ray strength shown in Figs. 4 and 5, i.e., either the Oslo data or the (γ,γ') data, both supplemented by the Gogny HFB plus QRPA predictions [21,23] outside the measured range, the reverse radiative neutron capture cross sections are now estimated with the TALYS reaction code [19] and compared with experimental cross sections

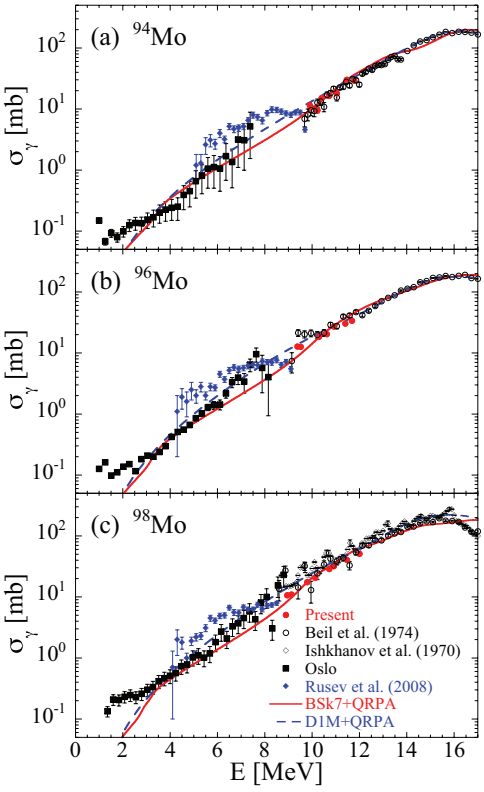

FIG. 4. (Color online) Comparison between the measured photoabsorption cross sections derived from photoneutron experiments (including ours) [17,18] as well as particle-γ coincidence measurements [8,25] (see also text for the corresponding error bars) and (γ,γ') data [24] for three Mo isotopes, ^{94}Mo (a), ^{96}Mo (b), and ^{98}Mo (c). Predictions from Skyrme HFB + QRPA (based on the BSk7 interaction) [20] and axially deformed Gogny HFB + QRPA models (based on the D1M interaction) [23] are also included.

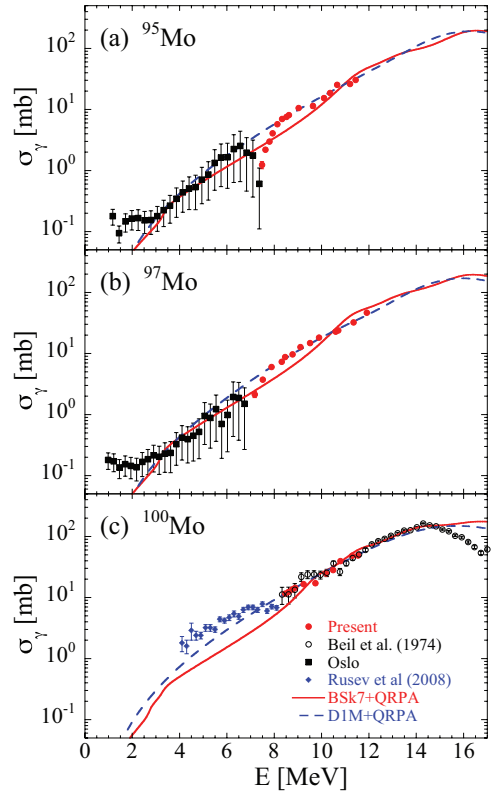

FIG. 5. (Color online) Same as Fig. 4 for ^{95}Mo (a), ^{97}Mo (b), and ^{100}Mo (c) isotopes for which the present (γ,n) data are available and either the particle-γ or the (γ,γ') data.

in Fig. 6. In addition to the $E1$ strength function which, in the energy range of relevance here, is essentially taken from experimental data, the TALYS calculation also depends on the adopted nuclear level density. We have used here the HFB plus combinatorial model of Ref. [34] normalized to exactly the same D_0 value and corresponding error bars, as those used to determine the γSF from the Oslo data (see Table I). Note that no uncertainty analysis has been performed when use is made of the (γ,γ') data, the systematic experimental error bars being most probably underestimated, as discussed above.

As can be seen in Fig. 6, the TALYS calculation agrees well with experimental data, which shows that within the uncertainties affecting the experimental γSF and D_0 value, all γSF data are compatible with both the photoabsorption and radiative capture channels, despite the fact that, as shown in Fig. 4, discrepancies exist between the different measurements. In the ^{95}Mo$(n,\gamma)^{96}$Mo, the larger ^{96}Mo γSF determined by photon scattering clearly leads to larger neutron capture cross sections.

The γSF method can now be applied to the experimentally unknown cross sections, namely ^{93}Mo$(n,\gamma)^{94}$Mo and ^{99}Mo$(n,\gamma)^{100}$Mo. While experimental information exists on the $E1$ strength function, no experimental D_0 data at the neutron binding energy can guide the nuclear level density models. For this reason, different D_0 values are adopted for ^{94}Mo, as given in Table I, and different level density models [35,36] considered to estimate their impact on the final cross section. Considering uncertainties affecting the experimental γSF (see Figs. 4 and 5) and theoretical ones affecting nuclear level densities, we have estimated the final upper and lower limits of the cross sections, as shown in Fig. 7. For the ^{99}Mo$(n,\gamma)^{100}$Mo cross section, the error bars only rely on the (γ,γ') data (with relatively small error bars) since there has been no particle-γ coincidence measurements yet for ^{100}Mo; this explains why smaller error bars are found in this case.

The resulting cross sections are also compared with the Japanese JENDL-4.0, American ENDF/B-VII.1, and Russian ROSFOND-2010 evaluations [37] in Fig. 7. While our ^{99}Mo$(n,\gamma)^{100}$Mo estimate is in good agreement with previous evaluations, our ^{93}Mo$(n,\gamma)^{94}$Mo cross section clearly does not

TABLE I. Adopted range of values for the average resonance spacings D_0 (in eV) and average γ-width $\langle\Gamma_\gamma\rangle$ (in meV).

Nucleus	$D_0^{\rm rec}$	$D_0^{\rm min}$	$D_0^{\rm max}$	$\langle\Gamma_\gamma\rangle^{\rm rec}$	$\langle\Gamma_\gamma\rangle^{\rm min}$	$\langle\Gamma_\gamma\rangle^{\rm max}$
^{94}Mo	81	57	105	213	149	277
^{95}Mo	831	582	1080	169	118	220
^{96}Mo	66.1	63.1	69.1	188	186	190
^{97}Mo	661	463	859	138	96	180
^{98}Mo	47	41	53	163	130	196

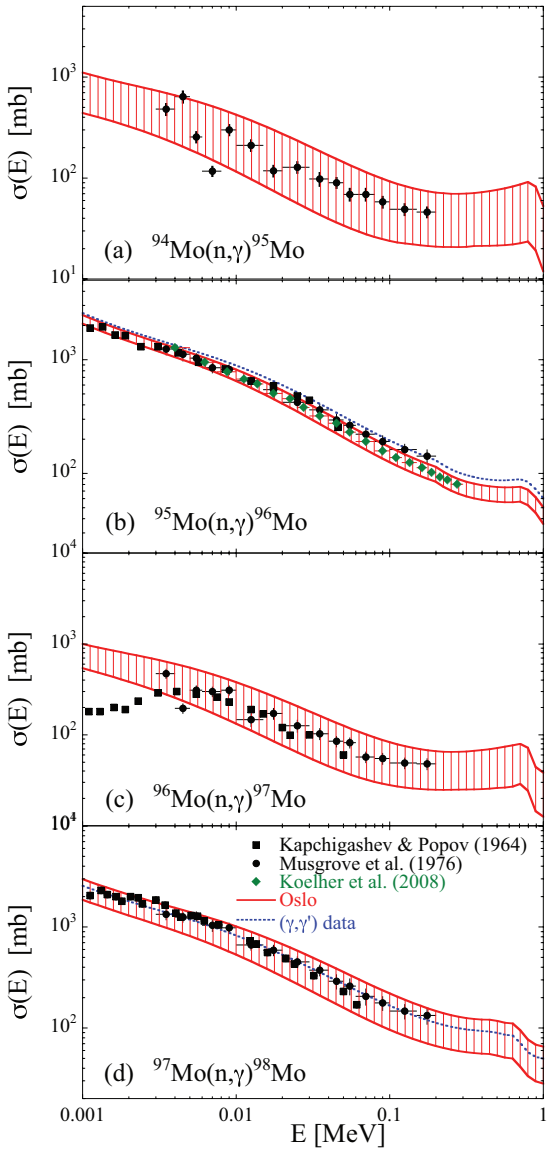

FIG. 6. (Color online) Comparison between the measured radiative neutron capture cross sections for ^{94}Mo (a), ^{95}Mo (b), ^{96}Mo (c), and ^{97}Mo (d) [30,32,33] with TALYS calculation making use of the D1M + QRPA calculation for the $E1$ strength supplemented either with the Oslo or the (γ,γ') data, as given in Figs. 4 and 5. See text for more details.

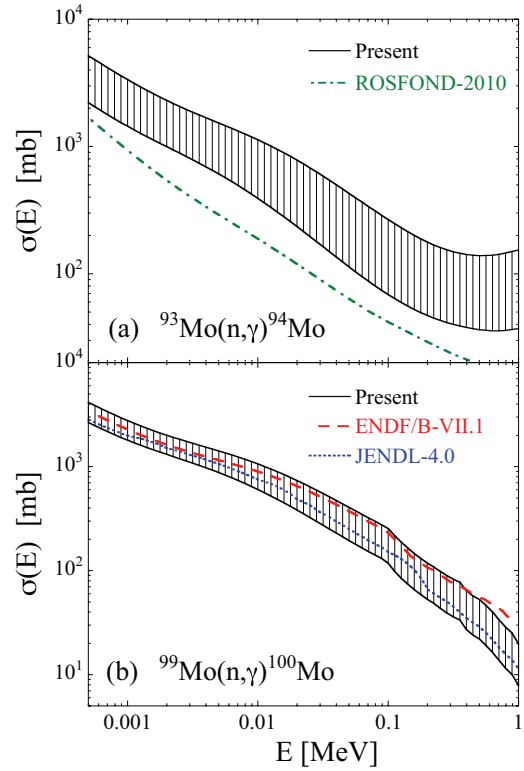

FIG. 7. (Color online) TALYS predictions for the radiative neutron capture cross sections of ^{93}Mo$(n,\gamma)^{94}$Mo (a) and ^{99}Mo$(n,\gamma)^{100}$Mo (b) making use of the Oslo or the (γ,γ') data whenever available. The error bands include uncertainties in the experimental γSF as well as the theoretical nuclear level densities. The dotted, dashed, and dash-dot curves correspond to the Japanese JENDL-4.0, American ENDF/B-VII.1, and Russian ROSFOND-2010 evaluations [37], respectively, whenever available.

agree with the Russian evaluation despite the non-negligible error bars. The resulting Maxwellian-averaged cross sections of astrophysical interest amount, at 30 keV, to 380 ± 200 mb for ^{93}Mo$(n,\gamma)^{94}$Mo and 410 ± 130 mb for ^{99}Mo$(n,\gamma)^{100}$Mo. Our ^{99}Mo$(n,\gamma)^{100}$Mo estimate (and consequently, also the ENDF/B-VII.1 and JENDL-4.0 ones) is found to be significantly larger than the theoretical cross sections of 240 ± 40 mb recommended in Ref. [38].

V. CONCLUSION

We have completed a systematic measurement of photoneutron cross sections for stable Mo isotopes with $A = 94$–100 using quasi-monochromatic laser-Compton γ-ray beams. In the context of the γSF method, we have investigated the γ-ray strength function that interconnects (γ,n) and (n,γ) cross sections within the statistical reaction model. We get a reasonable agreement with the experimental photoneutron and radiative neutron-capture cross sections for the Mo isotopes, using the Gogny HFB + QRPA model of $E1$ strength supplemented with experimental data that have been obtained by photon scattering or particle-γ coincidence data from $(^3\mathrm{He},\alpha\gamma)$ and $(^3\mathrm{He},^3\mathrm{He}'\gamma)$ reactions.

The new and accurate determination of the s-wave spacing for ^{96}Mo shows that in this specific case, there is a strong coherence between the different measurements, be it for the γSF in ^{96}Mo or the photoneutron and radiative neutron capture cross sections. Some discrepancies are still found between the (γ,γ') and particle-γ coincidence techniques, but accurate D_0 and $\langle\Gamma_\gamma\rangle$ evaluation at the neutron binding energy may help to resolve such discrepancies and give a coherent picture of the reaction mechanism. The present method shows that it is possible to significantly reduce the uncertainties in the determination of the neutron-capture rates on unstable nuclei if the γ-ray strength function can be determined experimentally below and in the vicinity of the neutron threshold. This method could consequently improve the predictions relative to the

nuclear physics ingredients of relevance in the description of the branching points in the *s*-process nucleosynthesis. More implications on nucleosynthesis will be studied in a forthcoming paper.

ACKNOWLEDGMENTS

We thank R. Schwengner of the Forschungzentrum Rossendorf for lending us enriched ^{94,95,96,98,100}Mo samples for the present measurement. This work is supported by the Japan Private School Promotion Foundation and the Konan-ULB bilateral project. S.G. acknowledges the financial support of the "Actions de recherche concertées (ARC)" from the "Communauté française de Belgique" and from the F.N.R.S. A.C.L. and M.G. acknowledge financial support from the Research Council of Norway, project grant no. 205528. P.K. acknowledges financial support from the Research Council of Norway. We acknowledge the PRACE project support for the computer resources.

[1] H. Utsunomiya *et al.*, Phys. Rev. C **80**, 055806 (2009).
[2] H. Utsunomiya *et al.*, Phys. Rev. C **82**, 064610 (2010).
[3] M. Arnould and S. Goriely, Phys. Rep. **384**, 1 (2003).
[4] P. Mohr *et al.*, Phys. Lett. B **488**, 127 (2000).
[5] H. Utsunomiya *et al.*, Phys. Rev. C **67**, 015807 (2003).
[6] M. Arnould, S. Goriely, and K. Takahashi, Phys. Rep. **450**, 97 (2008).
[7] F. Käppeler, R. Gallino, S. Bisterzo, and W. Aoki, Rev. Mod. Phys. **83**, 157 (2011).
[8] M. Guttormsen *et al.*, Phys. Rev. C **71**, 044307 (2005).
[9] G. Rusev *et al.*, Phys. Rev. C **73**, 044308 (2006).
[10] G. Rusev *et al.*, Phys. Rev. C **77**, 064321 (2008).
[11] M. Erhard *et al.*, Phys. Rev. C **81**, 034319 (2010).
[12] P. E. Koehler *et al.*, Phys. Rev. C (to be published).
[13] H. Utsunomiya *et al.*, Phys. Rev. C **84**, 055805 (2011).
[14] H. Harada and Y. Sigetome, J. Nucl. Sci. Technol. **32**, 1189 (1995).
[15] H. Harada *et al.*, Nucl. Instrum. Methods Phys. Res. A **554**, 306 (2005).
[16] H. Utsunomiya *et al.*, Nucl. Instrum. Methods Phys. Res. A **548**, 455 (2005).
[17] H. Beil, R. Bergere, P. Carlos, A. Lepretre, A. De Miniac, and A. Veyssiere, Nucl. Phys. A **227**, 427 (1974).
[18] B. S. Ishkhanov, I. M. Kapitonov, E. V. Lazutin, V. S. Sopov, I. M. Piskarev, and G. Shevchenko, Sov. J. Nucl. Phys. **11**, 394 (1970).
[19] A. J. Koning, S. Hilaire, and M. Duijvestijn, in *Nuclear Data for Science and Technology*, edited by O. Bersillon *et al.* (EDP Sciences, Les Ulis, France, 2008)), p. 211.
[20] S. Goriely, E. Khan, and M. Samyn, Nucl. Phys. A **739**, 331 (2004).
[21] S. Péru and H. Goutte, Phys. Rev. C **77**, 044313 (2008).
[22] S. Goriely, S. Hilaire, M. Girod, and S. Péru, Phys. Rev. Lett. **102**, 242501 (2009).
[23] M. Martini, S. Hilaire, S. Goriely, A. J. Koning, and S. Péru, *Nuclear Data for Science and Technology* (Elsevier, New York, USA, 2013).
[24] G. Rusev, R. Schwengner, R. Beyer *et al.*, Phys. Rev. C **79**, 061302(R) (2009).
[25] A. C. Larsen and S. Goriely, Phys. Rev. C **82**, 014318 (2010)
[26] M. Wiedeking, L. A. Bernstein, M. Krtička, D. L. Bleuel, J. M. Allmond, M. S. Basunia, J. T. Burke, P. Fallon, R. B. Firestone, B. L. Goldblum, R. Hatarik, P. T. Lake, I-Y. Lee, S. R. Lesher, S. Paschalis, M. Petri, L. Phair, and N. D. Scielzo, Phys. Rev. Lett. **108**, 162503 (2012).
[27] A. Schiller, L. Bergholt, M. Guttormsen, E. Melby, J. Rekstad, and S. Siem, Nucl. Instrum. Methods Phys. Res. A **447**, 498 (2000).
[28] A. C. Larsen, M. Guttormsen, M. Krtička, E. Běták, A. Bürger, A. Görgen, H. T. Nyhus, J. Rekstad, A. Schiller, S. Siem, H. K. Toft, G. M. Tveten, A. V. Voinov, and K. Wikan, Phys. Rev. C **83**, 034315 (2011).
[29] R. Capote, M. Herman, and P. Oblozinsky *et al.*, Nucl. Data Sheets **110**, 3107 (2009).
[30] P. E. Koehler, J. A. Harvey, K. H. Guber, and D. Wiarda, PoS Conference Proceedings (2008), available at http://pos.sissa.it/archive/conferences/053/041.
[31] S. F. Mughabghab, *Atlas of Neutron Resonances* (Elsevier, Amsterdam, 2006).
[32] S. P. Kapchigashev and Yu. P. Popov, Joint Inst. for Nucl. Res., Dubna, Reports No. 1845, France (1964), p. 104.
[33] A. R. De L. Musgrove, B. J. Allen, J. W. Boldeman, R. L. Macklin, and R. R. Winters, Nucl. Phys. A **270**, 108 (1976).
[34] S. Goriely, S. Hilaire, and A. J. Koning, Phys. Rev. C **78**, 064307 (2008).
[35] A. J. Koning, S. Hilaire, and S. Goriely, Nucl. Phys. A **810**, 13 (2008).
[36] S. Hilaire, M. Girod, S. Goriely, and A. J. Koning, Phys. Rev. C **86**, 064317 (2012).
[37] Evaluated Nuclear Data Files, 2011, http://www-nds.iaea.or.at/exfor.htm.
[38] Z. Y. Bao, H. Beer, F. Käppeler, F. Voss, K. Wisshak, and T. Rauscher, At. Data Nucl. Data Tables **76**, 70 (2000).